An Upper Limb Exoskeleton for Physical Assistance

Advanced robotic

Ali ahmadi

Supervisor : Dr bahrami

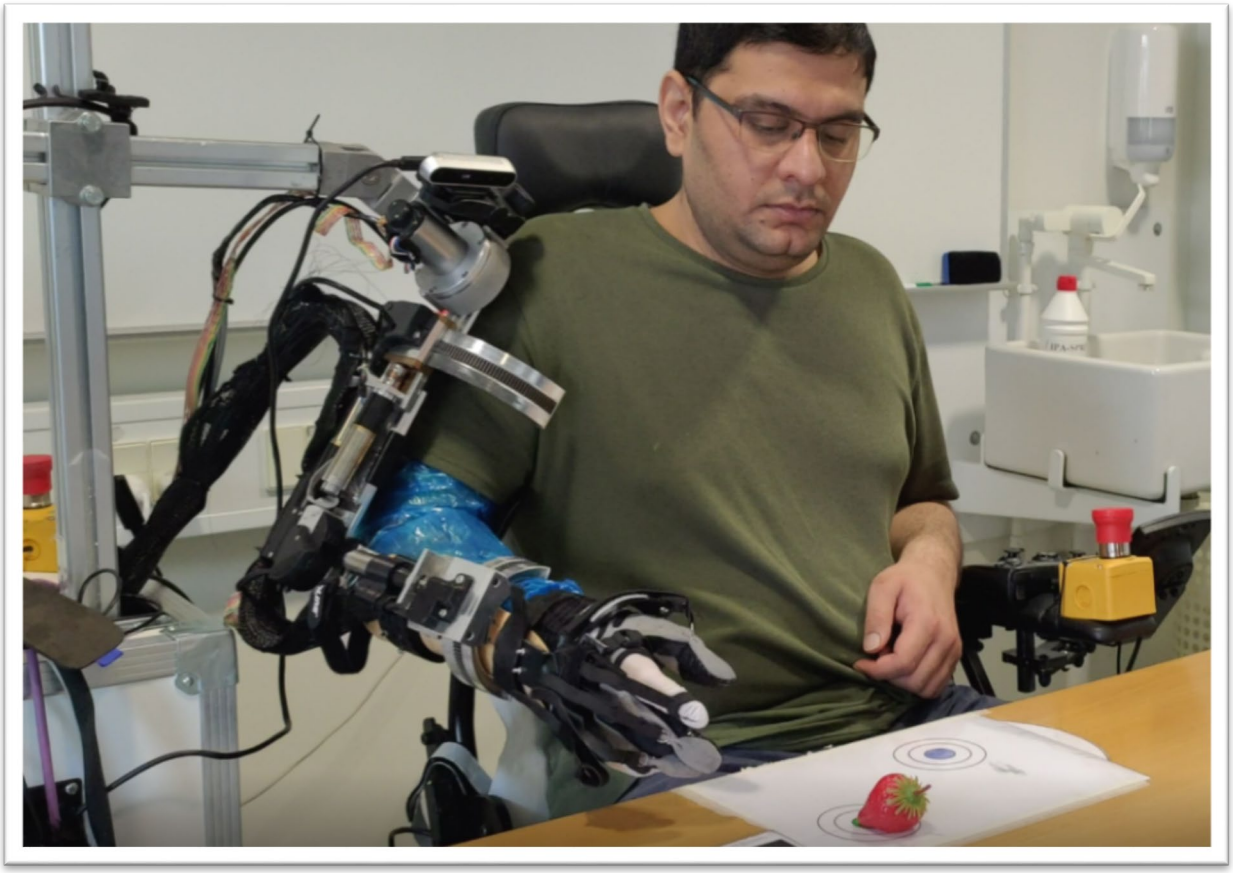

Objectives

Abstract: Wheelchair mounted upper limb exoskeletons offer an alternative way to support disabled individuals in their activities of daily living (ADL). Key challenges in exoskeleton technology include innovative mechanical design and implementation of a control method that can assure a safe and comfortable interaction between the human upper limb and exoskeleton. In this article, we present a mechanical design of a four degrees of freedom (DOF) wheelchair mounted upper limb exoskeleton. The design takes advantage of non-backdrivable mechanism that can hold the output position without energy consumption and provide assistance to the completely paralyzed users. Moreover, a PD-based trajectory tracking control is implemented to enhance the performance of human exoskeleton system for two different tasks. Preliminary results are provided to show the effectiveness and reliability of using the proposed design for physically disabled people.
Keywords: wheelchair upper limb exoskeleton robot; ADL assistance; PD control; dynamic modeling of an upper limb exoskeleton; trajectory tracking; wearable exoskeleton

1. Introduction

Cervical spinal cord injury (SCI) may result in incomplete or complete tetraplegia and lead to paralysis of all four extremities. Upper limb onset is one of the most profound impairments that significantly degrades the life of individuals with tetraplegia by compromising independence and social interactions. Moreover, it imposes a substantial financial burden on society in the long run. While advanced medical and surgical techniques, such as stem cell therapy, nerve transfer surgery, etc., have been used to restore the upper limb functionality, in some severe cases, it is hard to achieve desired results. Emerging technologies, such as assistive robots, can provide an alternative way to facilitate individuals with physical impairments in activities of daily living (ADL) [1,2] or therapeutic exercises [3,4]. During the past few decades, upper limb exoskeletons used for power amplification and rehabilitation have attracted intensive attention from the health care and engineering sectors [5]. However, given the utility and growing demand of exoskeletons for physical assistance, the technology still faces challenges in mechanical design, controls, and human–robot interaction. Of them, the mechanical design of a shoulder exoskeleton, including kinematic and kinetic analysis, is a major issue in developing an ergonomic system [6]. Christensen et al. [7] proposed a new three degrees of freedom (DOF) spherical mechanism to comply with the human glenohumeral joint movements. The proposed mechanism takes advantage of the double parallelogram (DPL) mechanism, which connects two revolute joints to achieve a spherical workspace and maintains a remote center of motion (RCM).

The results from the biomechanical analysis of the DPL mechanism presented in [7] have shown its significance for the exoskeleton applications [1]. Similarly, Castro et al. [8] presented a novel 3-DOF curved scissor mechanism that connects two revolute joints. The proposed mechanism complies with the human shoulder movements by maintaining the instantaneous center of rotation. Since the above mechanisms can support complex shoulder movements and provide a singularity-free workspace, the passive internal rotation has made it difficult to use for individual with tetraplegia. Alternatively, several other designs, including fully active or hybrid mechanisms to comply with the shoulder anatomical movements, were proposed [9–12]. These exoskeletons support the full range of shoulder girdle movement by preserving the remote center of rotation, but their effects on supporting the physically impaired people in common ADL have not yet been evaluated [13].
Moreover, flexible and parallel mechanisms have also been investigated to reduce inertial problem, but their size and complexity remain issues to be further addressed. Apart from the shoulder exoskeletons, exoskeletons that can support human forearm [4,14–17] and wrist movements [18–20] were developed. Among the existing mechanisms, a direct drive method and a C-ring mechanism are commonly used to support human forearm extension/flexion movements and wrist rotation, as reported in [2,5,20,21].
The feasibility of using an upper limb exoskeleton cannot only be proved by its design. Selection of a control method for improved physical human–robot interaction (pHRI) is essential for successful implementation and user acceptance. Regarding the trajectory tracking problem, proportional-derivative (PD) and proportional-integral-derivative (PID) controllers have been widely investigated for the different types of exoskeletons. Ease of implementation without having prior knowledge of robot dynamics and an ability to independently tune the control parameters have made the PD/PID control method among the most widely used control schemes [22]. However, in the PID controller, an integrator usually reduces the bandwidth of a closed loop system and removes the steady state error caused by extensive disturbance and uncertainties. Alternatively, a high value of the integrator gain may compromise the transient performance and destroys the system's stability. Therefore, many robotic manipulators, including exoskeletons, use purely PD control or PD control with relatively small integral gain [1,22–24]. It is known that a PD

controller can guarantee a semi global asymptotic stability after appropriately tuning the gains [23,24].

Several studies have been conducted to modify the linear PID controller that can guarantee an asymptotic stability. For example, PD control with sliding mode compensation [25], PD-based fuzzy sliding mode control [1], PD control with neural compensation [22] and so on. It is well understood that the PD controller can guarantee the stability for the robotic manipulators, but the asymptotic stability cannot be achieved if the robot dynamic contains gravitational torque. The exoskeleton presented in this study is designed to safely support the user in their ADL, especially the C-ring mechanism designed for shoulder and wrist rotation and the worm gear used to drive the elbow joint exoskeleton to hold the output position without energy consumption because of its non-backdrivability [26]. Moreover, hard constraints in the joint mechanisms may not allow the users to move beyond the safety limits.

In this paper, we present a PD control in the joint space to control the four degrees of freedom (DOF) upper limb exoskeleton robot [2] and investigate its effect as an assistive device to support individuals with physical impairments of the upper limbs in a set of ADLs. The contribution of the article can be summarized as follows. 1. The proposed design can support the human upper limb musculoskeletal structure
in basic ADL by providing a kinematically safe and singularity-free workspace. The deign along with the PD control is able to provide a satisfactory tracking performance. It is hypothesized that the trajectory tracking for C-ring mechanism and worm gear mechanism is less prone to the variation in payload, weight of human arm, and exoskeleton due to its ability to hold the output position without energy consumption.

2. The integration of the upper limb exoskeleton with the CarbonHand glove (BioServo Technologies AB, Kista, Sweden) offers a new paradigm that not only supports the user in manipulation but facilitates them also in hand opening and closing. The experimental evaluation has shown that the proposed design with the PD control scheme is appropriate in performing several ADLs, such as eating/drinking.

The paper is organized as follows. The mechanical design of a wheelchair exoskeleton is presented in Section 2 together with the kinematic modeling required to fulfil the task requirements in operational space. The dynamic model of the upper limb exoskeleton along with the PD control scheme is presented in Section 3. Moreover, the PD controller implementation along with the experimental results on the wheelchair exoskeletons is illustrated in Section 4. Subsequently, a discussion on the exoskeleton performance and its potential future directions are presented in Section 5. The work is finally concluded in Section 6.

2. Upper Limb Exoskeleton Robot

2.1. Mechanical Design

This section presents a design of an adaptive 4-DOF upper limb wheelchair mounted exoskeleton that can actively support the wearer in performing their activities of daily living, such as eating and drinking. The exoskeleton was designed after carefully analyzing the human upper limb biomechanics. To reduce the complexity of the human biomechanics, several studies have modeled the human arm as 7 degrees of freedom kinematics system by enforcing the simplifications to the upper limb joints and segments [27]. However, we have noticed that the 4-DOF exoskeleton is sufficient for the most common ADLs and keeps the workspace of the human upper extremity intact.

The exoskeleton in Figure 1b is designed as an open-chain structure to replicate the anatomy of human right upper limb and provides a controllable assistive torque to each joint. To describe the design and complete functioning of a robotic exoskeleton, we have separated the design into three sub-modules, i.e., shoulder joint mechanism, elbow module and a wrist module.

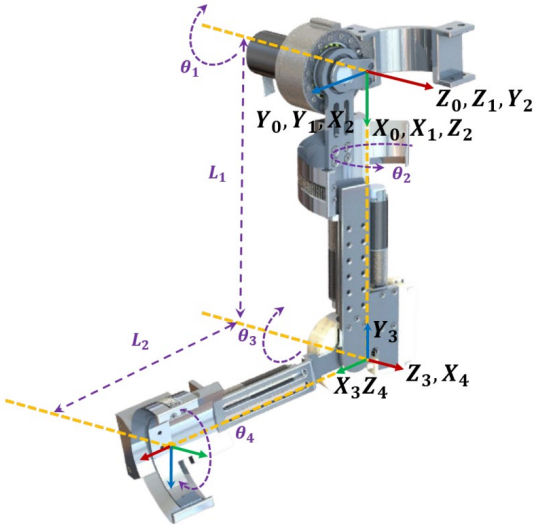

Figure 1 Overview of a 4-DOF wheelchair exoskeleton. (a) Mechanical model of 4-DOF upper limb exoskeleton.

The human shoulder (Glenohumeral) joint is modeled as a 3-DOF spherical joint that describes the orientation of the human upper arm. These three successive rotations are abduction/adduction, extension/flexion, and internal/external rotation. Hence, an open chain serial mechanism with three revolute joints whose axes of rotation intersect at a common point is kinematically equivalent to a spherical joint. Based on this observation, we have designed a shoulder mechanism that can actively support the 2-DOF glenohumeral joint movements such as shoulder extension/flexion movement and shoulder internal/external rotation, as shown in Figure 1a. The shoulder abduction/adduction movement is passively adjustable. Locking the upper arm abduction movement will prevent the user from moving beyond the wheelchair workspace, causing uncomfortable interaction with an external environment. The complete design of the shoulder mechanism,

shown in Figure 1a, is able to preserve the dynamic center of rotation throughout its workspace. The exoskeleton's extension/flexion is achieved by a direct drive brushless DC motor (EC-i40) and a CSD-17-80-2A-R harmonic drive to amplify the motor torque. A dovetail C-ring mechanism is used to actively support the human upper arm internal/external rotation. Furthermore, a 4 pole EC Maxon motor and a speed reducer drive the C-ring mechanism through a spur gear set.

The elbow joint module consists of a normal revolute joint. A Maxon EC-4 pole motor with a speed reducer located near the elbow joint controls the forearm extension/flexion through a worm gear set. The length of the exoskeleton's upper link is adjustable to adapt the user with different anthropomorphic parameters. Moreover, an upper arm support prevents the offset between the exoskeleton and human anatomical joints, i.e., shoulder and elbow joint, causing an uncomfortable interaction between the two systems. Finally, the wrist module consists of a C-ring mechanism that is designed to support the human wrist rotation (radial/ulnar deviation). A 4 pole EC Maxon motor and a speed reducer located along the forearm likewise actuate the C-ring of the wrist joint.

2.2. Kinematics

The kinematic model of the exoskeleton robot is developed by using Denavit–Hartenberg (DH) parameters defined in Table 1, where $L1$ and $L2$ represent the lengths of the upper arm and forearm links, respectively. Based on the DH parameters, the transformation matrix is given by

$$\mathrm{T}_{i-1,i} = \begin{bmatrix} c\theta_i & -s\theta_i c\alpha & s\theta_i s\alpha_i & a_i c\theta_i \\ s\theta_i & c\theta_i c\alpha_i & -c\theta_i s\alpha_i & a_i s\theta_i \\ 0 & s\alpha_i & c\alpha_i & d_i \\ 0 & 0 & 0 & 1 \end{bmatrix}$$

where s and c represent the sine and the cosine functions, respectively.

The forward kinematics is obtained by computing the overall matrix of transformation from the base frame to the wrist

Table 1. Denavit–Hartenberg (DH) parameters.

Joints	α_i	a_i	d_i	θ_i
1	$\pi/2$	0	0	$\pi/2-\theta_1$
2	$\pi/2$	0	L_1	$\pi+\theta_2$
3	$-\pi/2$	0	0	θ_3
4	0	0	L_2	θ_4

$$\mathrm{T}_{0,4} = \begin{bmatrix} m_{11} & m_{12} & m_{13} & n_{14} \\ m_{21} & m_{22} & m_{23} & n_{24} \\ m_{31} & m_{32} & m_{33} & n_{34} \\ 0 & 0 & 0 & 1 \end{bmatrix} \quad (2)$$

where all entries are given in the Appendix A.
The inverse kinematics is derived from the transformation matrix (2). The joint angles can be obtained as:

$$\begin{aligned}\theta_2 &= \pi + \arctan 2(n_{34}, n_{14}) \\ \theta_3 &= \pm \arcsin\left(\frac{n_{34}}{L_2 \sin\theta_2}\right) \\ \theta_1 &= \frac{\pi}{2} + \frac{1}{2} \arcsin \frac{n_{14} - n_{24}}{L_1 + L_2 \cos\theta_3 + L_2 \cos\theta_2 \sin\theta_3} \\ \theta_4 &= \arccos\left(\frac{m_{32}\cos\theta_2 + m_{31}\cos\theta_3 \sin\theta_2}{\cos^2\theta_2 - \cos\theta_3 \sin\theta_2}\right)\end{aligned} \tag{3}$$

2.3. Workspace and Singularity Analysis

The two most important properties that influence the geometrical design of a robotic exoskeleton are workspace and singularity analysis [28]. The kinematic model is used to analyze the workspace of the human upper limb and exoskeleton robot. Given the position of any point in the workspace, it is important to determine whether it belongs to the actual workspace or not, and helps to verify if at least one solution for the joint angles exists [2]. Therefore, a direct search method is employed to essentially evaluate the existence of an inverse kinematics solution for the human and robotic exoskeleton, shown in Figure 2b,c. The kinematic properties selected for this study are given in Appendix C.

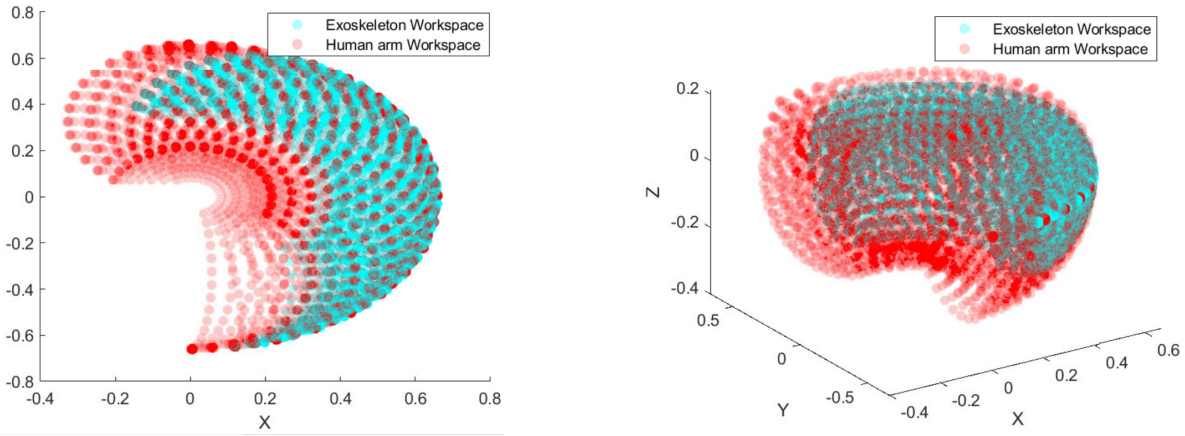

Figure 2 Workspace analysis of the 4-DOF upper limb exoskeleton (cyan) within the human arm workspace (red)

Apart from analyzing the reachable workspace, implementation of safe and stable operation is also required due to kinematic singularities within the workspace. Hence, it is necessary to identify all singular configurations while planning trajectories for the robotic exoskeleton. The manipulability ellipsoid and determinant of the Jacobian matrix are the two important indices that characterize the degree of singularity [29]. Our study determines the kinematic performance of the exoskeleton system by analyzing the manipulability index, which gives us information about the low and high manipulability regions, shown in Figure 2d,e.
In the manipulability analysis, we look at the position of the wrist only. Thus, we take Jacobian in the form of

$$\mathbf{J} = \frac{\partial \boldsymbol{n}}{\partial \boldsymbol{\theta}_i} = \begin{bmatrix} -n_{24} + L_1 c\theta_1 & -n_{34} c\theta_1 & -L_2(s\theta_1 s\theta_3 + c\theta_1 c\theta_2 c\theta_3) \\ n_{14} + L_1 s\theta_1 & -n_{34} s\theta_1 & L_2(c\theta_1 s\theta_3 - s\theta_1 c\theta_2 c\theta_3) \\ 0 & -L_2 c\theta_2 s\theta_3 & -L_2 s\theta_2 c\theta_3 \end{bmatrix} \quad (4)$$

2.3 inverse kinematics analisys

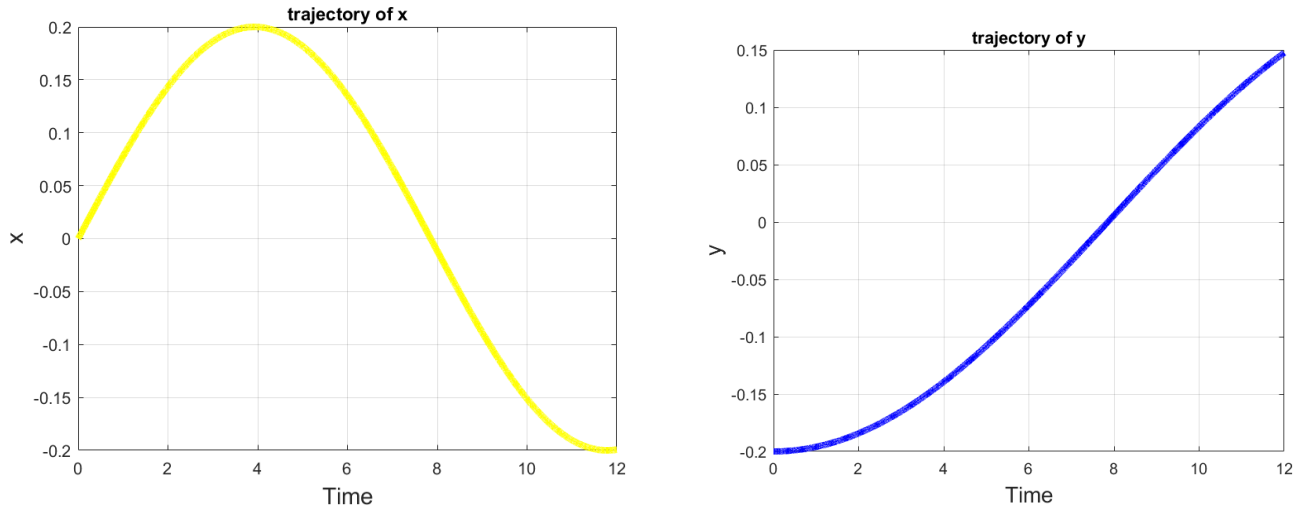

Figure 3 desired trajectory

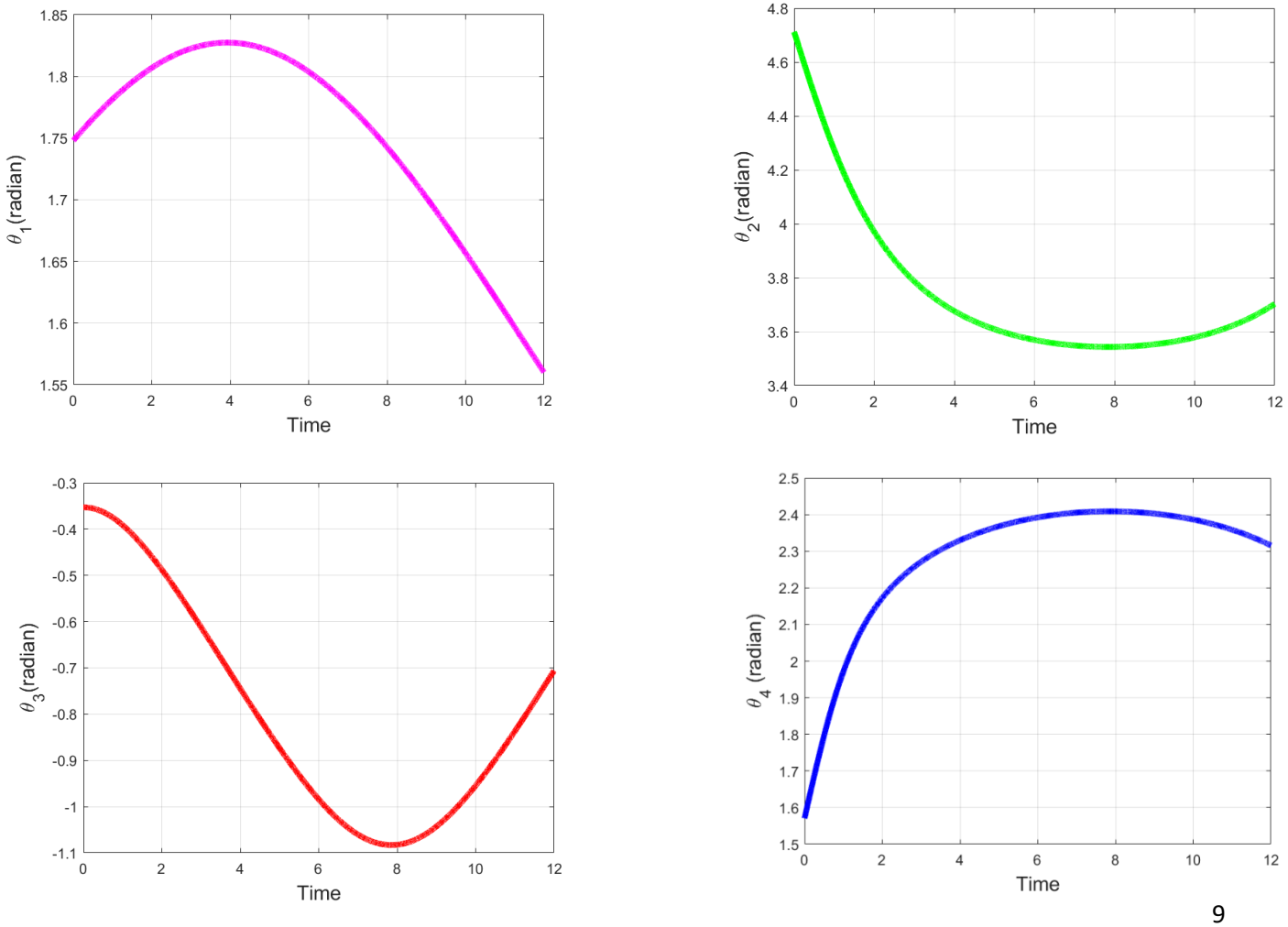

Figure 4 inverse kinematics solution

2.4 singularity analysis

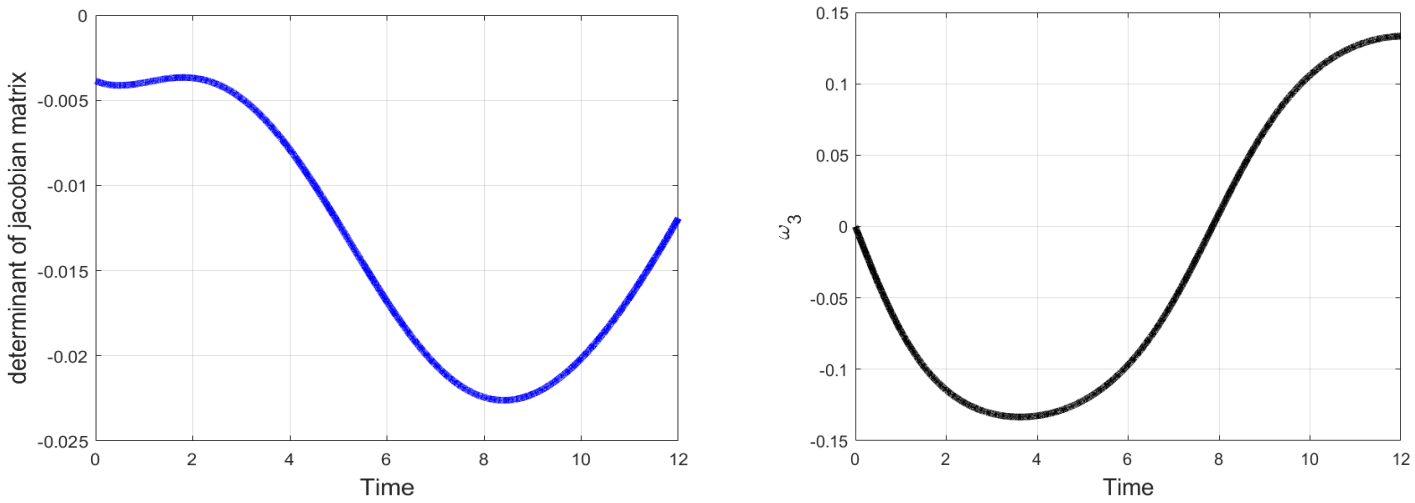

Figure 5 no singularity

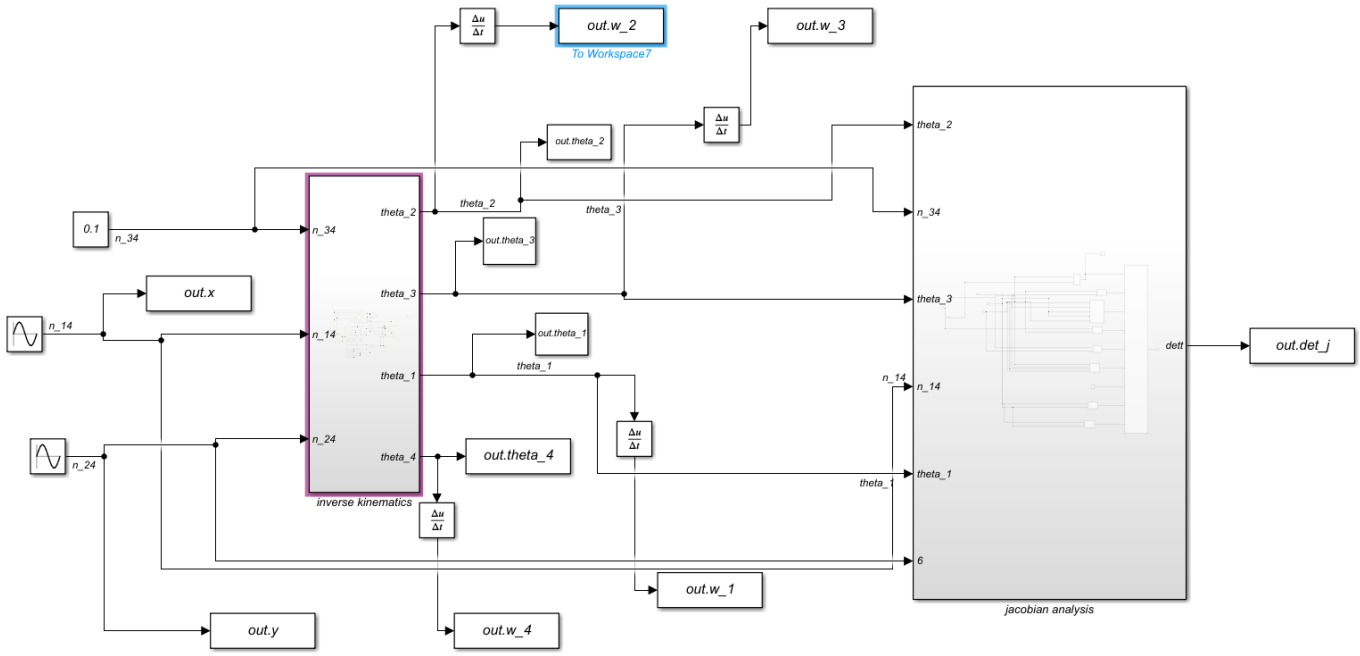

Figure 6 inverse kinematics and jacobian analysis

3.1Dynamics of manipulator

$$M(q)\ddot{q} + C(q,\dot{q})\dot{q} + \tau_g = \tau \qquad (6)$$

Table A1. Mechanical properties of the exoskeleton, and the average estimated anthropomorphic parameters for human subjects.

Link	Exoskeleton		Human Subject	
	Length (m)	Weight (kg)	Length (m)	Weight (kg)
Upper arm	0.33	2.5	0.33	1.386
Forearm	0.246	1.5	0.37	0.886

inertia matrix:

$$M_{11} = I_1 + L_1^2 m_3 + L_{c1}^2 m_1 + L_{c1}^2 m_2 + L_{c2}^2 m_3 c\theta_2{}^2 + L_{c2}^2 m_3 c\theta_3{}^2 + 2L_1 L_{c2} m_3 c\theta_3 - L_{c2}^2 m_3 c\theta_2{}^2 c\theta_3{}^2$$

$$M_{12} = L_{c2} m_3 s\theta_2 s\theta_3 (L_1 + L_{c2} c\theta_3) \qquad M_{23} = 0$$

$$M_{13} = -L_{c2} m_3 c\theta_2 (L_{c2} + L_1 c\theta_3) \qquad M_{31} = -L_{c2} m_3 c\theta_2 (L_{c2} + L_1 c\theta_3)$$

$$M_{21} = L_{c2} m_3 s\theta_2 s\theta_3 (L_1 + L_{c2} c\theta_3) \qquad M_{32} = 0$$

$$M_{22} = -m_3 L_{c2}^2 c\theta_3{}^2 + m_3 L_{c2}^2 + I_2 \qquad M_{33} = m_3 L_{c2}^2 + I_3$$

Coriolis forces:

$$C_1 = L_{c2} m_3 (L_1 \dot{\theta}_2^2 c\theta_2 s\theta_3 + L_1 \dot{\theta}_3^2 c\theta_2 s\theta_3 - 2L_1 \dot{\theta}_1 \dot{\theta}_3 s\theta_3 - L_{c2} \dot{\theta}_1 \dot{\theta}_2 s2\theta_2 - L_{c2} \dot{\theta}_1 \dot{\theta}_3 s2\theta_3$$
$$+ L_{c2} \dot{\theta}_2^2 c\theta_2 c\theta_3 s\theta_3 + 2L_1 \dot{\theta}_2 \dot{\theta}_3 c\theta_3 s\theta_2 + 2L_{c2} \dot{\theta}_2 \dot{\theta}_3 c\theta_3{}^2 s\theta_2 + 2L_{c2} \dot{\theta}_1 \dot{\theta}_2 c\theta_2 c\theta_3{}^2 s\theta_2 + 2L_{c2} \dot{\theta}_1 \dot{\theta}_3 c\theta_2{}^2 c\theta_3 s\theta_3)$$
$$C_2 = (L_{c2}^2 m_3 (-2c\theta_2 s\theta_2 \dot{\theta}_1^2 c\theta_3{}^2 + s2\theta_2 \dot{\theta}_1^2 + 4\dot{\theta}_3 s\theta_2 \dot{\theta}_1 c\theta_3{}^2 - 4\dot{\theta}_3 sin\theta_2 \dot{\theta}_1 + 2\dot{\theta}_2 \dot{\theta}_3 sin2\theta_3))/2$$
$$C_3 = (L_{c2} m_3 (2L_1 \dot{\theta}_1^2 s\theta_3 + L_{c2} \dot{\theta}_1^2 sin2\theta_3 - L_{c2} \dot{\theta}_2^2 s2\theta_3 + 4L_{c2} \dot{\theta}_1 \dot{\theta}_2 s\theta_2 - 2L_{c2} \dot{\theta}_1^2 c\theta_2{}^2 c\theta_3 s\theta_3 - 4L_{c2} \dot{\theta}_1 \dot{\theta}_2 c\theta_3{}^2 s\theta_2))/2$$

The torque due to gravity:

$$G_1 = L_1 m_3 s\theta_1 + L_{c1} m_1 s\theta_1 + L_{c1} m_2 s\theta_1 + L_{c2} m_3 c\theta_3 s\theta_1 - L_{c2} m_3 c\theta_1 c\theta_2 s\theta_3$$

$$G_2 = L_{c2} m_3 s\theta_1 s\theta_2 s\theta_3$$

$$G_3 = L_{c2} m_3 (c\theta_1 s\theta_3 - c\theta_2 c\theta_3 s\theta_1)$$

3.2 Inverse dynamic simulations

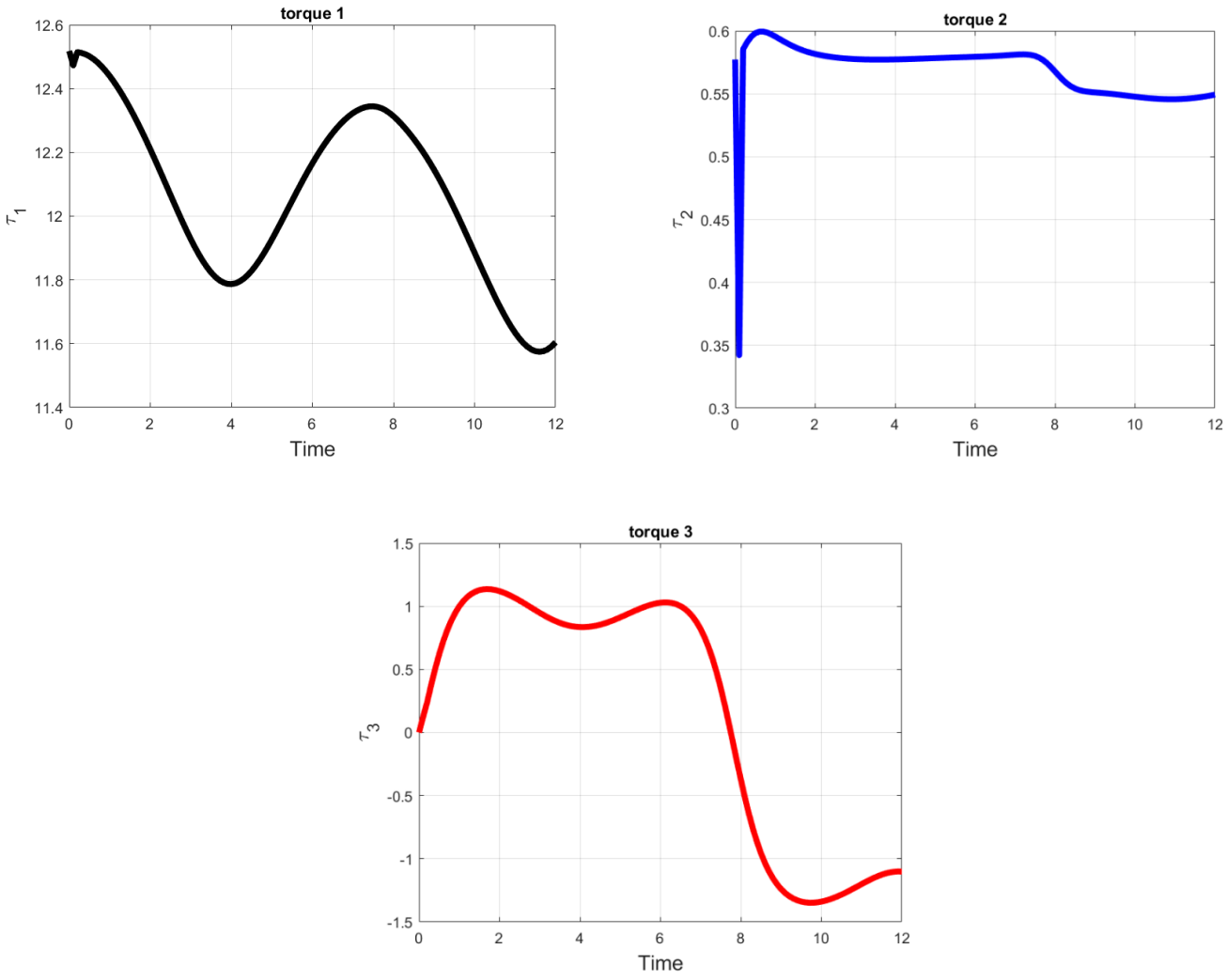

Figure 7 inverse dynamics

3.3 Inclusion of non-rigid body effects

It is important to realize that the dynamic equations we have derived do not encompass all the effects acting on a manipulator. They include only those forces which arise from rigid body mechanics. The most important source of forces that are not included is friction. All mechanisms are, of course, affected by frictional forces. In present-day manipulators, in which significant gearing is typical, the forces due to friction can actually be quite large—perhaps equaling 25% of the torque required to move the manipulator in typical situations.
In order to make dynamic equations reflect the reality of the physical device, it is important to model (at least approximately) these forces of friction. A very simple model for friction is viscous friction, in which the torque due to friction is proportional to the velocity of joint motion. Thus, we have

$$\tau_{friction} = \vartheta\dot{\theta}$$

where v is a viscous-friction constant. Another possible simple model for friction, Coulomb friction, is sometimes used. Coulomb friction is constant except for a sign dependence on the joint velocity and is given by

$$\tau_{friction} = c\ sgn(\dot{\theta})$$

These friction models are then added to the other dynamic terms derived from the rigid-body model, yielding the more complete model

$$\tau_{friction} = \vartheta\dot{\theta} + c\ sgn(\dot{\theta}) = F(\theta, \dot{\theta})$$

$$\boldsymbol{\tau = M\ddot{\theta} + C\dot{\theta} + \tau_g + F(\theta, \dot{\theta})}$$

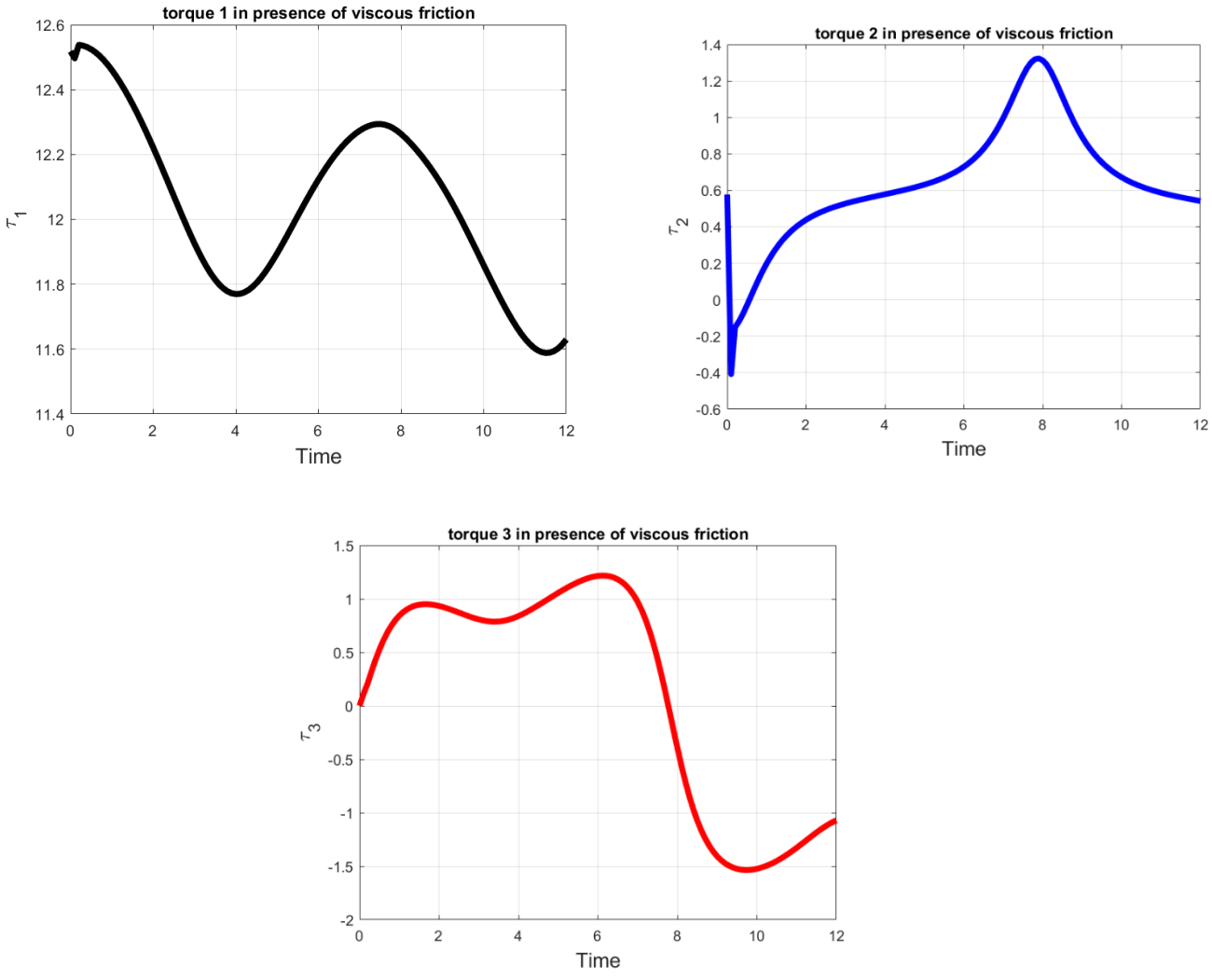

Figure 8 inverse dynamics in presence of friction

Appendix A

$$m_{11} = c\theta_4(s\theta_1 s\theta_3 + c\theta_1 c\theta_2 c\theta_3) - c\theta_1 s\theta_2 s\theta_4$$

$$m_{12} = -s\theta_4(s\theta_1 s\theta_3 + c\theta_1 c\theta_2 c\theta_3) - c\theta_1 c\theta_4 s\theta_2$$

$$m_{13} = c\theta_3 s\theta_1 - c\theta_1 c\theta_2 s\theta_3$$

$$m_{21} = -c\theta_4(c\theta_1 s\theta_3 - c\theta_2 c\theta_3 s\theta_1) - s\theta_1 s\theta_2 s\theta_4$$

$$m_{22} = s\theta_4(c\theta_1 s\theta_3 - c\theta_2 c\theta_3 s\theta_1) - c\theta_4 s\theta_1 s\theta_2$$

$$m_{23} = -c\theta_1 c\theta_3 - c\theta_2 s\theta_1 s\theta_3$$

$$m_{31} = c\theta_2 s\theta_4 + c\theta_3 c\theta_4 s\theta_2$$

$$m_{32} = c\theta_2 c\theta_4 - c\theta_3 s\theta_2 s\theta_4$$

$$n_{14} = L_2(c\theta_3 s\theta_1 - c\theta_1 c\theta_2 s\theta_3) + L_1 s\theta_1$$

$$n_{24} = -L_2(c\theta_1 c\theta_3 + c\theta_2 s\theta_1 s\theta_3) - L_1 c\theta_1$$

$$n_{34} = -L_2 s\theta_2 s\theta_3$$

References

1. Teng, L.; Gull, M.A.; Bai, S. PD-Based Fuzzy Sliding Mode Control of a Wheelchair Exoskeleton Robot. *IEEE/ASME Trans. Mechatronics* **2020**, *25*, 2546–2555. [CrossRef]
2. Thøgersen, M.; Gull, M.A.; Kobbelgaard, F.V.; Mohammadi, M.; Bengtson, S.H.; Struijk, L.N.A. EXOTIC-A Discreet User-Based
5 DoF Upper-Limb Exoskeleton for Individuals with Tetraplegia. In Proceedings of the 3rd International Conference on Mechatronics, Robotics and Automation (ICMRA), Shanghai, China, 16–18 October 2020; pp. 79–83.
3. Chaparro-Rico, B.D.M.; Cafolla, D.; Castillo-Castaneda, E.; Ceccarelli, M. Design of arm exercises for rehabilitation assistance.
J. Eng. Res. **2020**, *8, 204–218*. [CrossRef]
4. Zuccon, G.; Bottin, M.; Ceccarelli, M.; Rosati, G. Design and Performance of an Elbow Assisting Mechanism. *Machines* **2020**,
8, 107674. [CrossRef]
5. Gull, M.A.; Bai, S.; Bak, T. A review on design of upper limb exoskeletons. *Robotics* **2020**, *9*, 16. [CrossRef]
6. Delgado, P.; Alekhya, S.; Majidirad, A.; Hakansson, N.A.; Desai, J.; Yihun, Y. Shoulder Kinematics Assessment towards Exoskeleton Development. *Appl. Sci.* **2020**, *10*, 6336. [CrossRef]
7. Christensen, S.; Bai, S. Kinematic analysis and design of a novel shoulder exoskeleton using a double parallelogram linkage.
J. Mech. Robot. **2018**, *10*, 041008. [CrossRef]
8. Castro, M.N.; Rasmussen, J.; Andersen, M.S.; Bai, S. A compact 3-DOF shoulder mechanism constructed with scissors linkages
for exoskeleton applications. *Mech. Mach. Theory* **2019**, *132*, 264–278. [CrossRef]
9. Kim, B.; Deshpande, A.D. An upper-body rehabilitation exoskeleton Harmony with an anatomical shoulder mechanism: Design,
modeling, control, and performance evaluation. *Int. J. Robot. Res.* **2017**, *36*, 414–435. [CrossRef]
10. Hsieh, H.; Chen, D.; Chien, L.; Lan, C. Design of a Parallel Actuated Exoskeleton for Adaptive and Safe Robotic Shoulder
Rehabilitation. *IEEE/ASME Trans. Mechatronics* **2017**, *22*, 2034–2045. [CrossRef]
11. Hunt, J.; Lee, H.; Artemiadis, P. A novel shoulder exoskeleton robot using parallel actuation and a passive slip interface. *J. Mech. Robot.* **2017**, *9*, 011002. [CrossRef]

12. Huamanchahua, D.; Vargas-Martinez, A.; Ramirez-Mendoza, R. Kinematic of the Position and Orientation Synchronization of the
Posture of an DoF Upper-Limb Exoskeleton with a Virtual Object in an Immersive Virtual Reality Environment. *Electronics* **2021**,
10, 1069. [CrossRef]
13. Galofaro, E.; D'antonio, E.; Patané, F.; Casadio, M.; Masia, L. Three-Dimensional Assessment of Upper Limb Proprioception via a
Wearable Exoskeleton. *Appl. Sci.* **2021**, *11*, 2615. [CrossRef]
14. Zahedi, A.; Wang, Y.; Martinez-Hernandez, U.; Zhang, D. A wearable elbow exoskeleton for tremor suppression equipped with
rotational semi-active actuator. *Mech. Syst. Signal Process.* **2021**, *157*, 107674. [CrossRef]
15. Li, Z.; Bai, S. Design and Modelling of a Compact Variable Stiffness Mechanism for Wearable Elbow Exoskeletons, In Proceedings
of the 7th International Conference on Control, Mechatronics and Automation (ICCMA), Delft, The Netherlands, 6–8 November
2019; pp. 342–346.
16. Li, Z.; Chen, W.; Zhang, J.; Bai, S. Design and control of a 4-DOF cable-driven arm rehabilitation robot (CARR-4). In Proceedings
of the IEEE International Conference on Cybernetics and Intelligent Systems (CIS) and IEEE Conference on Robotics, Automation
and Mechatronics (RAM), Ningbo, China, 19–21 November 2017; pp. 581–586.
17. Chaparro-Rico, B.; Cafolla, D.; Ceccarelli, M.; Castillo-Castaneda, E. Design and simulation of an assisting mechanism for arm
exercises. In *Advances in Italian Mechanism Science*; Springer: Vicenza, Italy, 2017; pp. 115–123.